Integration of a Shunt Active Filter and Energy Storage to Energy Quality Improvement in Distributed Power Systems

Francisco Kelson Pereira Alves
Universidade Federal do Ceará
Sobral, Ceará, Brasil
fkelsonpa@alu.ufc.br

Lucivando Ribeiro de Araújo
Universidade Federal do Ceará
Sobral, Ceará, Brasil
lucivandoribeiro@yahoo.com.br

Isaac Rocha Machado
Universidade Federa do Ceará
Sobra, Ceará, Brasil
isaacmachado@gmail.com

Vandilberto Pereira Pinto
Universidade Federal do Ceará
Sobral, Ceará, Brasil
vandilberto@yahoo.com.br

Larissa Souza Pereira
Universidade Federal do Ceará
Sobral, Ceará, Brasil
laris.sal@hotmail.com

***Abstract*— The increase of renewable energy generation has caused a significant increase of current harmonics and degradation of the energy quality in distribution systems. This paper presents the study and modeling of a Shunt Active Filter (SAPF) integrated with an Energy Storage System (ESS) applied in energy quality improvement. The distribution system consists of non-linear loads, wind generation and a SAPF integrated to an ESS (batteries bank) through the DC link. The objective is to perform, at the same time, the harmonic currents filtering and the low frequency oscillating power elimination inserted by the loads-generation group. The SAPF power circuit consists of a six-pulse Voltage Source Converter (VSC) and the control implemented from the instantaneous powers measurement of the load-generation group. The batteries bank is connected to the SAPF DC link through a bidirectional DC/DC converter and its control is implemented by the grid active power measuring. In this way, the ESS control has the objective of applying load leveling to the loads and distributed generation set.**

Keywords*— *Harmonics, storage, filtering, batteries, converter

I. INTRODUCTION

The increase of the nonlinear loads makes more expressive the presence of current harmonics in the Electric Power Systems (EPS). The tendency is that the harmonic injection is intensified, since the micro and mini generation from intermitent sources requires an electronic converter in grid connected systems. This continuous change proposes the great challenge of maintaining the EPS operating within the minimum energy quality standards.

A very versatile way of current harmonics filtering is the use of SAPFs, which have valuable advantages over passive filters such as the fact that there are no resonances with grid and also the capacity of selective harmonics filtering [2]. It can also be used for reactive power compensation, and also the possibility to operate integrated with ESS. Aiming at the efficient use of energy from intermitent sources and also preventive action against grid overload, the storage technologies are today an important research tool aimed at micro grids energy quality improvement.

In order to propose a solution to all these energy quality problems, being able to implement harmonic current compensation, and at the same time, to use energy storage for load leveling, this paper presents a study of the integration of SAPF and ESS controls. Basically it involves using a six-pulse Voltage Source Converter (VSC) to perform the required current compensation and a two-quadrant DC/DC converter responsible for the charge and discharge ESS connected to a common DC link. Fig. 1 presents an overview of the simulated EPS and the simplified control scheme.

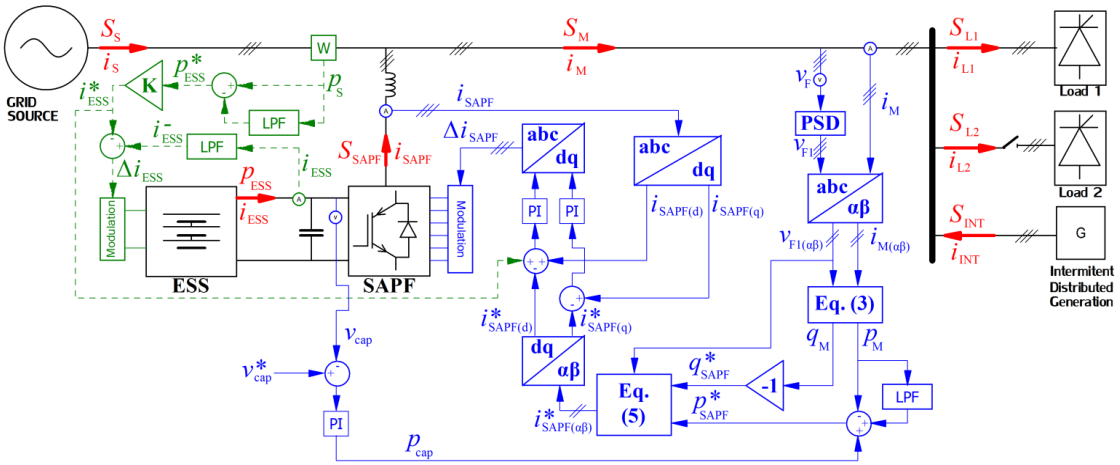

Fig. 1. Overview of simulated distributed power system

In Fig. 1 it is observed that the total power of the micro grid (S_M) ()is the sum of the load demands (S_{L1} and S_{L2}) and the distributed wind generation (S_{Int}). Due to the intermitent characteristic, the active power p_M must vary widely, which in most cases causes poor energy quality, especially when the distribution grid is not robust enough to absorb such intermittency. The idea of this paper is that load leveling is done, ensuring that the total power supplied by the grid(S_S) is smoothed and as constant as possible.

Ideally only the currents fundamental components should flow in the principal grid. The SAPF current, i_{SAPF}, is the sum of two components: $i_{ESS(1)}$, referring to active power flow between the ESS and the Common Coupling Point (CCP); and $i_{M(H)}$, referring to harmonic and reactive powers compensation of the load-generation set. Similarly, i_M is sum of. two components: $i_{M(1)}$, referring to the active power flow and $i_{M(H)}$, referring to the non-active power flow of the load-generating set.

The objective of this work is to verify the performance of the ESS and SAPF acting in an integrated way. An integrated methodology is used, where SAPF and ESS controls share parameter information. While the SAPF acts on harmonic current compensation, the ESS acts to smooth the active power flow between the main grid and the load-generation set.

The SAPF control can basically be done in two ways: the direct (traditional) method where the currents are of the load-generation set (i_M) are effectively measured for the calculation and selection of the compensation powers, and indirect method, where the main grid currents (i_S) are measured and control is done by the energy balance in DC link. The direct method has the advantage of performing a more efficient filtering and more robust control and therefore is chosen in this work.

Using the direct method it is possible to compute the compensation currents through the instantaneous power theory concepts, which is based on the instantaneous power calculation in the αβ reference frame [1]. The control loops are implemented with the use of three PI controllers: two PI controllers for the currents loops (the current control loops are made in dq reference frame) and one for the DC link voltage control loop.

The drive of the ESS converter is based on monitoring the active power flow of the main grid (p_s), whose purpose is to minimize the intermittencies inserted by the load-generation set. The control of the ESS converter is performed by comparing between the measured oscillating grid power and its filtered value (a low-pass filter is used).

II. Instantaneous Power Theory

The instantaneous power theory is based on the instantaneous powers active, p, and reactive, q, calculation in coordinates αβ, hence also called pq theory. The abc coordinate system is represented in an analogous way in the αβ coordinates using the Clark transform. Considering a three-phase system with voltages v_a, v_b and v_c, the respective voltages v_α and v_β are given by:

$$\begin{bmatrix} v_\alpha \\ v_\beta \end{bmatrix} = \sqrt{\frac{2}{3}} \begin{bmatrix} 1 & -\frac{1}{2} & -\frac{1}{2} \\ 0 & \frac{\sqrt{3}}{2} & -\frac{\sqrt{3}}{2} \end{bmatrix} \begin{bmatrix} v_a \\ v_b \\ v_c \end{bmatrix} \quad (1)$$

It is important to note that Eq. (1) is power invariant, that is, the power in the αβ plane is the same as in the abc plane. The transformation matrix above has the orthogonality property, where its inverse is equal to the transpose of the same. Therefore, the inverse relation of Eq. (1) is given by the following transformation:

$$\begin{bmatrix} v_a \\ v_b \\ v_c \end{bmatrix} = \sqrt{\frac{2}{3}} \begin{bmatrix} 1 & 0 \\ -\frac{1}{2} & \frac{\sqrt{3}}{2} \\ -\frac{1}{2} & -\frac{\sqrt{3}}{2} \end{bmatrix} \begin{bmatrix} v_\alpha \\ v_\beta \end{bmatrix} \quad (2)$$

Eqs. (1) and (2) can also be used analogously for currents transformation. The instantaneous active and reactive powers are given by:

$$\begin{bmatrix} p \\ q \end{bmatrix} = \begin{bmatrix} v_\alpha & v_\beta \\ -v_\beta & v_\alpha \end{bmatrix} \begin{bmatrix} i_\alpha \\ i_\beta \end{bmatrix} \quad (3)$$

The active and reactive instantaneous powers can be represented by their oscillating and constant components, where:

$$\begin{bmatrix} p \\ q \end{bmatrix} = \begin{bmatrix} \bar{p} + \tilde{p} \\ \bar{q} + \tilde{q} \end{bmatrix} \quad (4)$$

$\bar{p}$ and $\tilde{p}$ being the active and oscillating active power components, respectively. Analogously, $\bar{q}$ and $\tilde{q}$ represent the constant and oscillating reactive power components, respectively. The SAPF control is done through the application of the concepts above, as presented in the following topics.

III. SAPF Control Theory

The SAPF control diagrams are shown in Fig. 1 with continuous lines, and will be detailed in the following topics.

A. Positive Sequence Detector (PSD)

The reference voltages for the compensating currents calculation must not contain distortions, which justifies the use of the positive sequence detector. In this way just the fundamental voltage component is used in the instantaneous powers calculation.

B. Instantaneous power caculations (p^*_{SAPF}, q^*_{SAPF})

The instantaneous powers calculation is made from the voltages and currents in the *αβ* reference frame, as presented in section 2. After this calculation, the average and oscillating components of the active and reactive powers are obtained with the aid of low-pass filters. Finally, the powers used in the currents references calculation are chosen. Usually, $\tilde{p}$ and q.

C. Currents compensation calculation ($i^*_{SAPF(\alpha\beta)}$)

Knowing the charge-generation set currents (i_M) and the positive sequence PCC voltages (v_{FI}), the compensation currents are calculated through the *pq* theory. At first, the Clark transform is applied, according to Eq. (1), obtaining the voltages and currents in the *αβ* plane ($v_{F1(\alpha\beta)}$ and $i_{M(\alpha\beta)}$, respectively). Using Eq. (3), the active and reactive instantaneous powers (p_M e q_M) are calculated. The average and oscillating parts of the powers are obtained with the aid of Low-Pass Filters (LPF). $\tilde{p}$ and q are chosen for the compensation currents calculation.

The power p_{cap} represents the switching losses and DC link losses. p_{cap} is obtained from the DC link voltage control loop. Again, from Eq. (3):

$$\begin{bmatrix} i^*_{SAPF(\alpha)} \\ i^*_{SAPF(\beta)} \end{bmatrix} = \frac{1}{\Delta}\begin{bmatrix} v_{F1(\alpha)} & v_{\beta F1(\beta)} \\ v_{F1(\beta)} & -v_{F1(\alpha)} \end{bmatrix}\begin{bmatrix} p^*_{SAPF} \\ q^*_{SAPF} \end{bmatrix} \quad (5)$$

Where:

$$\Delta = v^2_{F1(\alpha)} + v^2_{F1(\beta)} \quad (6)$$

D. Current control loop

Initially the compensating currents ($i^*_{SAPF(\alpha\beta)}$) and the SAPF measured currents (i_{SAPF}) are transformed to the *dq* synchronous reference frame by the Park transformation. After transforming, the currents are compared and the error is directed to the PI controller, as shown in Fig. 1. It is possible to verify that there is communication between the SAPF and ESS controls via the reference current i^*_{ESS}.

The concepts presented in [3] suggest a method for tuning the K_{pi} and K_{ii} gains of the controllers. It is established that these gains must satisfy the following expression for the currentsi_d and i_q

$$\frac{di_d}{dt} = \frac{di^*_d}{dt} + K_p\tilde{\imath}_d + K_i\int \tilde{\imath}_d\, dt \quad (7)$$

$$\frac{di_q}{dt} = \frac{di^*_q}{dt} + K_p\tilde{\imath}_q + K_i\int \tilde{\imath}_q\, dt \quad (8)$$

Where:

$$\tilde{\imath}_d = (i^*_d - i_d) \text{ e } \tilde{\imath}_q = (i^*_q - i_q) \quad (9)$$

Deriving Eq. (7) and (8) is the dynamic closed loop current error defined by Eq. (10) and (11), respectively.

$$\frac{d\tilde{\imath}^*_d}{dt} + K_{pi}\frac{d\tilde{\imath}_d}{dt} + K_{ii}\tilde{\imath}_d = 0 \quad (10)$$

$$\frac{d\tilde{\imath}^*_q}{dt} + K_{pi}\frac{d\tilde{\imath}_q}{dt} + K_{ii}\tilde{\imath}_q = 0 \quad (11)$$

Passing Eq. (10) and (11) to the frequency domain gives a second-order equation to each. It is known that the generic form of this equation is:

$$s^2 + 2\zeta\omega_{ni}s + \omega^2_{ni} \quad (12)$$

Therefore, it is established that:

$$K_{pi} = 2\zeta\omega_{ni} \quad (13)$$

$$K_{ii} = \omega^2_{ni} \quad (14)$$

Where ζ and ω_{ni} represent the desired damping coefficient and natural frequency. The latter must be sized for the highest possible value, but limited by the switching frequency. In this case, the damping coefficient chosen was $\sqrt{2}/2$.

E. DC link control loop

The link voltage cc (v_{cap}) changes due to oscillating active power circulation and must therefore be continuously regulated. This adjustment is made through the parameter p_{cap}, obtained from the use of a PI controller, as shown in Fig. 1.

The gains K_{pv} e K_{iv} can be obtained in a way analogous to the procedure adopted in the current loop. In the *dq* reference frame:

$$C_{Link}\frac{dv_{cap}}{dt} = C_{Link}\frac{dv^*_{cap}}{dt} + K_{pv}\tilde{v}_{cap} + K_{iv}\int v_{cap}\, dt \quad (15)$$

Where:

$$\tilde{v}_{cap} = (v^*_{cap} - v_{cap}) \quad (16)$$

Deriving Eq. (15):

$$\frac{d\tilde{v}^*_{cap}}{dt} + \frac{K_{pv}}{C_{Link}}\frac{d\tilde{v}_{cap}}{dt} + \frac{K_{iv}}{C_{Link}}\tilde{v}_{cap} = 0 \quad (17)$$

Again, by analogy with the generic form of the second-order characteristic equation, proportional and integral gains are calculated by:

$$K_{pv} = 2\zeta\omega_{nv}C_{Link} \quad (18)$$

$$K_{iv} = \omega^2_{nv}C_{Link} \quad (19)$$

Where ω_{nv} is the natural frequency of the DC link voltage loop, and must be set to values below the grid frequency.

IV. ESS Modeling and Control

For the ESS, a DC/DC converter was used that operates in two quadrants, allowing the flow of current (and power) in two directions. The following topics detail the ESS power and control circuits.

A. ESS power circuit

Fig. 2 presents the ESS converter topology.

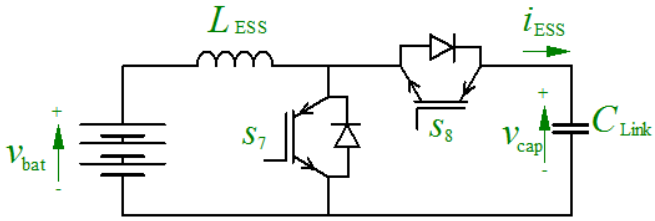

Fig. 2. ESS power converter.

The inductor L_{ESS} allows to control the average voltage (V_{S_7}) on the switch S_7, so that it is directly proportional to the DC link voltage (v_{cap}) by duty cycle (D) product. That is:

$$V_{S_7} = Dv_{cap} \quad (20)$$

The i_{ESS} current is given by:

$$i_{ESS} = \frac{V_{S_7} - v_{bat}}{R_{bat}} \quad (21)$$

Therefore, it is possible to control the current flow between the DC bus and the batteries bank via the D adjustment.

Since the principal objective is to maintain the grid power constant, the ESS must absorb energy when the load-generation power demand is reduced (*D* must increase until $V_{S_7} > v_{cap}$), otherwise, when the load-generation power demand is increased the ESS must supply power to the system (*D* must decrease until $V_{S_7} < v_{cap}$). Therefore, to

allow two-way power flow, it was established that:

$$v_{bat} = \frac{v_{cap}}{2} \tag{22}$$

B. Power flow control

As shown in Fig. 1 with discontinuous lines, the energy to be supplied or absorbed from the DC bus is obtained by measured grid power and its filtered value.

By comparing the measured grid power with its filtered value, p^*_{ESS} is obtained. This power reference value is converted into the current reference value i^*_{ESS} through gain K and later compared to the average battery bank current. The average battery bank current is obtained with the aid of an LPF, since its waveform is pulsed.

C. Batteries bank modeling

The concepts presented in [12] were used as reference for modeling the batteries. It is considered a source of dependent voltage v in series with the equivalent resistance R_{bat}, according to Fig. 3:

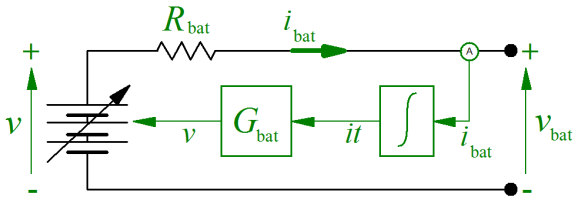

Fig. 3. Battery Schematic

The block G_{bat} corresponding to the mathematical model of the voltage v as a function of the integral of the current i_{bat}. This mathematical function allows an approximation of the charge state of the battery. Fig. 4 shows a typical discharge curve of battery:

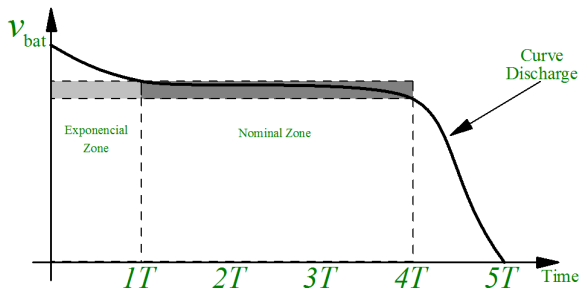

Fig. 4. Battery Discharge Curve

Through Eq. (23) it is possible to reproduce the curve shown in Fig. 4.

$$G_{bat} = v_0 - k\frac{Q}{Q - it} + Ae^{(-B \cdot it)} \tag{23}$$

Where:

v_0 = batteries constant voltage (V);

k = polarization voltage (V);

Q = storage capacity (Ah);

A = amplitude of exponential zone (V);

B = inverse time constant of exponential zone $(Ah)^{-1}$;

R_{bat} = internal resistance (Ω);

First, the two parameters of the exponential area must be calculated as follows:

$$A = v_{máx} - v_{exp} \tag{24}$$

$$B = \frac{3}{Q_{exp}} \tag{25}$$

Where the parameters $v_{máx}$, v_{exp} and Q_{exp} are respectively: the maximum voltage, minimum voltage and the energy of the exponential zone. After establishing the above parameters, it is possible to calculate the constant k by Eq. (26):

$$k = \frac{[v_{máx} - v_{nom} + Ae^{((-BQ_{nom})-1)}](Q - Q_{nom})}{Q_{nom}} \tag{26}$$

Where v_{nom} and Q_{nom} are nominal parameters of voltage and energy. The equivalent internal resistance can be scaled by the following expression:

$$R_{bat} = v_{nom}\frac{1 - \eta}{0{,}2 \cdot Q_{nom}} \tag{27}$$

The η equals the average battery efficiency. Eq. (26) allows to find an adequate resistance value when not enough information is available on this parameter [12].

V. SIMULATIONS

To analyze the performance of the proposed integration system, the PSCAD / EMTDC software was used. The system parameters used in the simulations are presented in Table 1. It is desired to observe through the simulations the following main points:

1. Correction in waveform and reduction in current THD;
2. Control and filtering of active and reactive power in the Network;
3. DC link voltage control and battery model performance.

TABLE I. SYSTEM PARAMETERS

Names of Parameters	***Values of Parameters***
Phase Voltage, e frequency	v_F = 220V (rms), f = 60 Hz
SAPF Parameters	L_{SAPF} = 0,8mH, C_{LINK} = 2,5mF
ESS Parameters	L_{ESS} = 5mH
Voltage Link CC	v_{cap} = 900V
Nominal Power of Loads 1 and 2	S_{L1} = 15kVA, S_{L2} = 7,5kVA
Loads THDs 1 and 2	THD = 28%, both
Nominal Voltage Batteries	v_{bat} = 450V
Batteries Model Parameters	A = 5 V, B = 1,2 $(Ah)^{-1}$, K = 2,2V, Q = 10 Ah
Frequency and control	ω_{ni}=4000π(*rad/s*), ω_{nv}=10π (*rad/s*)

Due to software limitations the analysis time was set at 5 seconds (sec). The dynamics of the system is analyzed through 7 state changes exposed below:

In 0.0 sec: The load 1 fed by the network is driven by a three-phase rectifier (cc-converter) controlled by thyristors whose modulation causes a 30° delay in the triggering of the switches. Therefore, in addition to injecting harmonics in the network causing a distortion of 28% in the current (Fig. 5), and the power factor is also affected getting in about 0.87 for a total power of 15kVA;

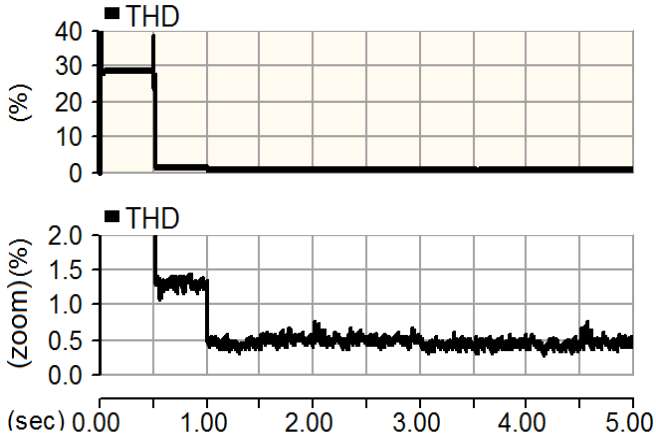

Fig. 5 – Current Source THD

In 0.5 sec: The active filter is activated and passes current filtering in the network. The current THD is reduced from 28% to about 1.3% (see Fig. 5). The change in the waveform of the currents in the network is shown in Fig. 6 at the very moment when the SAPF is triggered in 0.5 seconds.

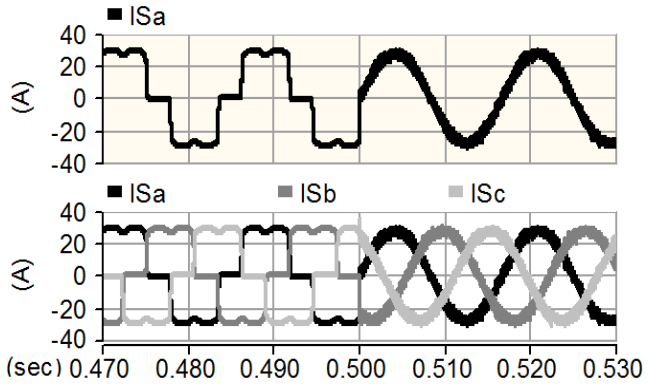

Fig. 6 – Currents Source before and after of triggering the SAPF

It can be seen in Fig. 7 that SAPF acts as a non-active power source. This power that previously circulated in the network, and now only in the filter. Thus, the network only provides active power, raising the power factor and reducing the total power demand. The small increase that occurs in the active power demand of the network derives from the switching losses in the SAPF.

In 1.0 sec: The ESS is activated and from then on it controls the oscillations of power demand in the Network. The storage system performs filtering to ensure constant active power. It is also possible to verify a greater reduction in THD (Fig. 5) after activating it.

In 1.5 sec: The second load, also nonlinear, is triggered. It can be seen in Fig. 7 that this new power demand is filtered by ESS (active power) and SAPF (non-active power).

In 2.0 sec: An intermitent distributed source will inject active and reactive power into the system. In the Fig. 7, it is seen that the intermitent active power oscillates between 3kW and 5kW, the intermitent reactive power is around 0.5kW.

In 3.0 sec: The second load is switched off, and the ESS starts to absorb the intermitent power surplus.

In 4.0 sec: the intermitent source is stalled.

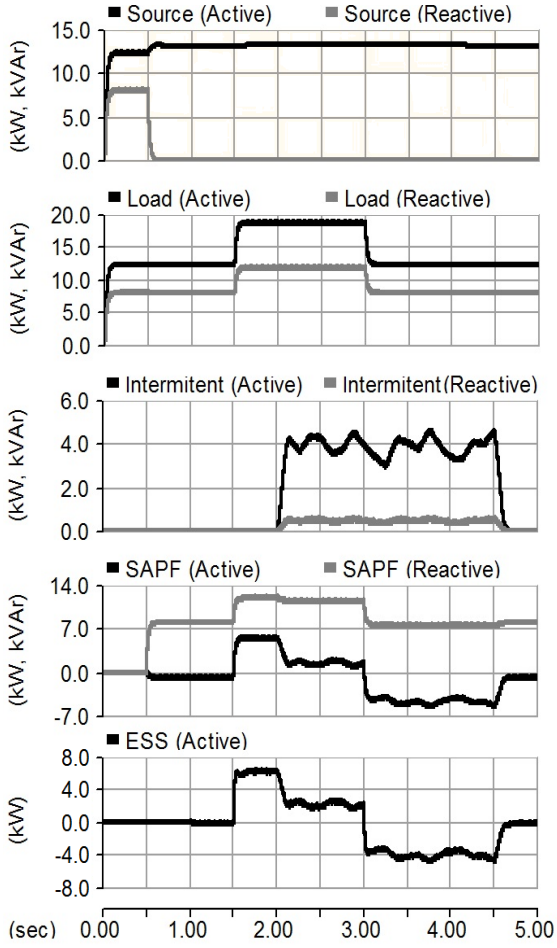

Fig. 7 - Active and Reactive Powers (Source, Load, Intermitent, SAPF, ESS).

Each time a system change is made, the DC Link voltage varies as seen in Fig. 8. The maximum variation of this voltage (Vcap) was about 23V, and occurs at 1.5s when the second load is driven. The analysis time of the simulations does not allow to verify a significant discharge in the battery due to its high storage capacity (Q = 10 Ah).

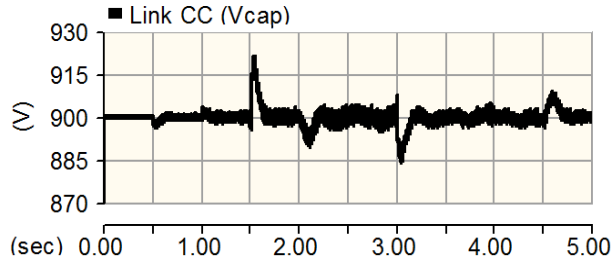

Fig. 8 – Voltage of Link CC

From Fig. 9 it can be seen that its operating voltage did not reach the exponential zone, as explained in Fig. 4.

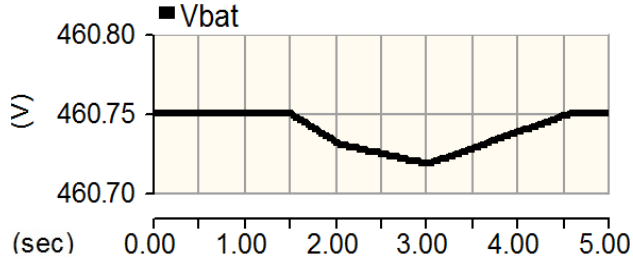

Fig. 9 – Batteries Voltage of ESS

VI. Conclusions

In this article, it was possible to verify all the versatility of active filters in distributed generation systems. Integrating the storage system in addition to improving SAPF performance helps reduce power demands. The parameters of Table 1 showed good results, thus validating the calculations and theories used. The direct compensation method and the voltage and current controllers presented good dynamics and stability. The simulations clearly show the results of the objectives outlined: 1 - large reduction of current THD; 2 - active and reactive power flow control; 3 - Link cc control and validation of modeling parameters and battery performance.

Acknowledgment

The authors acknowledge Coordenação de Aperfeiçoamento de Pessoal de Nível Superior (CAPES), Conselho Nacional de Desenvolvimento Cientifico e Tecnológico (CNPq) and Universidade Federal do Ceará (UFC) *campus* Sobral for the support to this work.

References

[1] M. A. Hirofumi Akagi, Edson Hirokazu Watanabe, *Instantaneous Power Theory and Applications to Power Conditioning*. IEEE Press, Wiley-Interscience, A John Wiley & Sons, Inc., Publication, 2007.

[2] Kaushal R. Chaudhari, Tapan A. Trivedi, *Analysis on Control Strategy of Shunt Active Power Filter for Three-phase Three-wire System,* LDRP-ITR, KSV University, Electrical Engineering Department, Gandhinagar, India, 2014.

[3] N. Mendalek, K. Al-Haddad, F. Fnaiech and L.A. Dessaint, *Nonlonear Control Technique to Enhance Dynamic Performance of a Shunt Active Power Filter*, IEE Proc.-Electr. Power Appl., Vol. 150.

[4] Ricardo L. A. Ribeiro, Christian C. de Azevedo, Raphaell M. de Sousa, *A Robust Adaptive Control Strategy of Active Power Filters for Power-Factor Correction, Harmonic Compensation, and Balancing of Nonlinear Loads,* IEEE Transactions On Power Electronics, Vol. 27, No. 2, February 2012.

[5] M. I. M. Montero, E. R. Cadaval, F. B. González, *Comparison of Control Strategies for Shunt Active Power Filters in Three-Phase Four-Wire Systems,* IEEE Transactions On Power Electronics, Vol. 22, No. 1, January 2007.

[6] SILVA, F.J.G. *Estudo do Chaveamento por Vetores Espaciais em Modulação por Largura de Pulso em Conversores Multiníveis.* Dissertação (Mestrado em Engenharia Elétrica) – Universidade Federal do Rio de Janeiro/COPPE, Rio de Janeiro, 2008. 130 f.

[7] J. S. OMORI, *Aplicação de Filtro Ativo Trifásico em Sistemas de Distribuição de Baixa Tensão*. Dissertação (Mestrado em Engenharia Elétrica e Informática Industrial) – Universidade Tecnológica Federal do Paraná, Campus Curitiba, 2007. 201 f.

[8] RASHID, M. H. *Eletrônica de Potência: Circuitos, Dispositivos e Aplicações*. 2. ed. São Paulo: Makron Books, 1999. 819 p.

[9] M.J. Newman, D.N. Zmood, D.G. Holmes, *Stationary Frame Harmonic Reference Generation for Active Filter Systems*. Department of Electrical and Computer Systems Engineering, Monash University, Australia, 2002.

[10] Bojoi, R.I., et all, *Current Control Strategy for Power Conditioners Using Sinusoidal Signal Integrators in Synchronous Reference Frame*, IEEE Transactions On Power Electronics, Vol. 20, No. 6, November 2005.

[11] Mattavelli, P., *A Closed-Loop Selective Harmonic Compensation for Active Filters*, IEEE Transactions On Power Electronics, Vol. 37, No. 1, January/February 2001.

[12] Tremblay, O.; Dessaint, L.-A.; Dekkiche, A.-I.; , "A Generic Battery Model for the Dynamic Simulation of Hybrid Electric Vehicles," *Vehicle Power and Propulsion Conference, 2007. VPPC 2007. IEEE* , vol., no., pp.284-289, 9-12 Sept. 2007.